Nanoscale

PAPER

View Article Online
View Journal | View Issue

Cite this: *Nanoscale*, 2025, **17**, 8642

Atomic force microscopy as a multimetrological platform for energy devices

Hüsnü Aslan, *[a] Khaled Kaja,†[b] José Morán-Meza,[b] François Piquemal,[b] José Alvarez, [c,d] Nicolas Chauvin, [e] José Penuelas, [e] Steffan Møller Sønderskov[a] and Philippe Regreny[e]

Received 4th December 2024,
Accepted 5th March 2025

DOI: 10.1039/d4nr05107f

rsc.li/nanoscale

In this article, we present a comprehensive study utilizing atomic force microscopy (AFM) as a multimetrological platform for the characterization of novel energy harvesting devices, with a particular focus on optical nanomaterials – nanowires. Despite their challenging structure, AFM offers exceptional versatility in probing the dimensional and functional properties of nanowires at the nanoscale. We demonstrate the capabilities of AFM measurements to provide an extensive understanding of the structural, electrical, and spectroscopic properties of nanowires using different operational modes, including electrostatic force microscopy (EFM), Kelvin probe force microscopy (KPFM), and conductive-AFM (C-AFM). Our findings establish AFM as an invaluable metrological tool for the development of cutting-edge energy harvesting technologies and optical nanomaterials.

1. Introduction

Nanotechnology has revolutionized the field of materials science, enabling the development of novel energy harvesting devices and nanomaterials with unique properties at the nanoscale. Owing to their one-dimensional structure, nanowires have emerged as highly promising candidates for improved-efficiency devices in solar and electro-mechanical energy applications. When vertically aligned in solar cells, semiconducting nanowires expose a larger surface area for light collection than their film-like counterparts. Similarly, in electro-mechanical transducers vertical nanowires exhibit a favoured configuration for mechanical bending, implying higher energy conversion efficiency. Thus, these optical nanomaterials are excellent candidates for diverse biomedical and environmental applications.

To fully utilize the scientific and commercial potential of nanowires, a comprehensive understanding of their properties is required. However, accurate characterization is complicated due to their nanoscale geometry, fragility, and complex behaviour. Atomic force microscopy (AFM) has emerged as a powerful metrological tool capable of probing surface properties and obtaining dimensional information with high resolution, precision and accuracy using low, controllable forces.[1] Its versatility and ability to operate in various modes make it an ideal platform for investigating nanowires and advancing their associated technological applications.

AFM's scanning capabilities allow for precise imaging and measurement of nanowires' dimensions, providing crucial insights into their morphology, roughness and aspect ratio. For instance, AFM was employed to measure the diameter and length of silicon nanowires (NWs), unveiling their growth kinetics in line with their mechanical and structural properties.[2] Various AFM-based techniques were utilized to study the surface roughness of nanowires, which plays a crucial role in their electronic and mechanical properties.[3] Wang *et al.* investigated the surface roughness of zinc oxide nanowires, revealing the influence of growth conditions on their surface morphology and potential for device applications.[4]

Despite the importance of nanowires' surface morphology, investigating their electrical properties plays a key role in the development of their energy-conversion functionalities. Conductive-AFM (C-AFM) and electrostatic force microscopy (EFM) have been used to comprehend the electrical properties of nanowires. On the one hand, C-AFM, using a continuous contact approach, measures local variations in conductivity and current distribution along nanowires, aiding in the assessment of their local electronic transport properties.[5,6] EFM, on the other hand, uses a non-contact

[a]*Dansk Fundamental Metrologi (DFM) – Danish National Metrology Institute, Hoersholm, Denmark. E-mail: asl@dfm.dk*
[b]*Laboratoire national de métrologie et d'essais (LNE), FR-78197 Trappes Cedex, France*
[c]*Université Paris-Saclay, CentraleSupélec, CNRS, Laboratoire de Génie Électrique et Électronique de Paris, Gif-sur-Yvette, France*
[d]*Sorbonne Université, CNRS, Laboratoire de Génie Électrique et Électronique de Paris, Paris, France*
[e]*Ecole Centrale de Lyon, CNRS, INSA Lyon, Université Claude Bernard Lyon 1, CPE Lyon, INL, UMR5270, Ecully 69130, France*
† Present address: Bruker Nano Surfaces & Metrology, Karlsruhe, Germany.

approach for measuring electrical properties related to charge distributions and local oxidation effects.[7–9] EFM was utilized to study the charge distribution of copper nanowires, highlighting the influence of surface charges on their electrical behaviour.[10] Similar to EFM, Kelvin probe force microscopy (KPFM) has been employed to investigate the work function and surface potential of nanowires, enabling a comprehensive understanding of their electronic properties. Singh *et al.* characterized single-crystalline germanium nanowires using KPFM, revealing the influence of crystal orientation on their surface potential.[11]

Furthermore, AFM-based characterization in the radiofrequency (RF) range (not shown here) uses scanning microwave microscopy (SMM) or scanning microwave impedance microscopy (sMIM) methods to investigate the local electrical and dielectric properties of NWs. SMM and sMIM use a conductive AFM probe to transmit a microwave signal (in the gigahertz frequency range) to the sample of interest and to collect the signal reflected by the sample. They enable impedance or admittance measurements at the nanoscale, giving access to the electrical permittivity (dielectric constant and loss angle tangent) and dopant concentration of various materials (semiconductors, dielectrics, 2D materials, quantum materials, *etc.*).[12–18] Li *et al.* investigated the dopant distribution profiles of Si (n-type) and Zn (p-type) impurities within individual multijunction GaAs NWs using qualitative sMIM measurements and correlated with infrared scattering-type near-field optical microscopy.[19]

In this paper, we demonstrate that AFM can serve as a versatile and indispensable tool for the multimetrological characterization of nanowires and novel energy harvesting devices. We show results obtained on semiconducting NWs using various operational modes and complementary techniques, demonstrating precise dimensional measurements, electrical property mapping, and spectroscopic analysis under various environmental conditions. This thorough understanding of nanowire properties paves the way for the development and optimization of nanoscale energy harvesting devices, contributing to advancements in the field of nanotechnology.

2. Materials and methods

2.1. AFM metrology

Dimensional characterization at the micro- and nanoscale is routinely conducted using calibrated AFMs traceable to certified length standards. Once calibrated in the *x*, *y*, and *z* directions (see Fig. 1), the AFM can be used for metrological purposes. AFMs comprise a head unit and a sample stage, which can move independently from each other. They can be used either in tip-scanning or sample-scanning configurations. Moreover, AFM operations can be conducted through various approaches based on the feedback mechanism. Typically, three different methods are used for imaging, namely, contact mode with deflection-based feedback, intermittent contact mode with amplitude modulation and deflection feedback, and non-contact mode with either amplitude or frequency modulation feedback. Furthermore, force–distance or force–time feedback methods can be used for dynamic nanomechanical microscopy (DNM), while current or contact potential feedback can be used for conductive-AFM measurements. Lastly, AC and DC bias feedback methods can be used for nanoelectrical measurements such as EFM and KPFM. When using AFM beyond imaging, two or more feedback mechanisms are employed simultaneously, for example in C-AFM, while deflection feedback helps measure the surface topography and ensures reliable contact for charge transport, the current feedback is used to measure the resistance/conductivity of the surface. Often each method has distinct advantages and disadvantages, for example, the contact mode is an excellent choice for hard, flat surfaces and is essential for any current and thermal measurements, but on soft samples this method likely will damage the sample and the tip. AFM, as a multi-metrological platform, enables swift changes between modes and various feedback methods to capitalize on the advantages of each mode while overcoming or compensating for their inherent limitations.

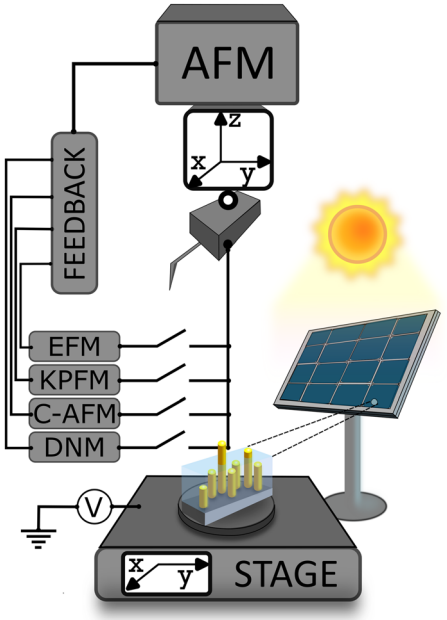

Fig. 1 Schematic of the AFM with its calibrated *x*, *y*, *z* scanner head and its *x*, *y* moving sample stage, as a multi-metrological platform with both tip-scan and sample-scan configurations as well as many modes for nanoelectrical and mechanical characterization.

2.2. Semiconducting nanowires

The fabrication of novel photovoltaic semiconductor-based energy harvesting devices aims at maximizing the effective surface area of light-exposed tuneable nanostructures while ensuring that they preserve their delicate form. Here, we fabri-

cate III–V nanowires tailored for integration in solar cells, using different configurations as follows.

2.2.1. Pure and doped GaAs nanowires. Arrays of pure and doped GaAs nanowires (NWs) were fabricated by molecular beam epitaxy (MBE) on silicon (111) substrates using the Vapor–Liquid–Solid (VLS) growth method.[20,21] The first step consisted of gently cleaning the substrate in acetone and ethanol, followed by a 200 °C outgassing for a few minutes to remove contaminants. Subsequently, the substrate was introduced into the main chamber for further growth, where its temperature was increased to 450 °C to deposit Ga liquid droplets on the surface for etching the silica native layer. Then, the substrate temperature was increased to ~600 °C to initiate the VLS growth by simultaneously opening the Ga and As shutters. The crystal structure can be finally tuned by adjusting the V/III ratio, which was set close to 2.4 in our case, resulting in a cubic crystalline structure. By tuning the growth time, we were able to control the length of the nanowires, and their diameters were modified by stopping the VLS growth to switch to a radial growth mode (Fig. 2).

The NW doping was controlled by evaporating a foreign element during the growth, *i.e.*, Be for p-type doping and Te for n-type doping. Generally, the dopant concentration is expected to be somehow linearly dependent on the dopant molecular beam flux during the VLS growth. However, the dopant incorporation process is rather complex since it induces a pathway related to the dopant's incorporation in the liquid catalyst droplet, followed by diffusion and nucleation at the liquid–solid interface.

A series of vertical, p-doped and n-doped NWs were grown and then encapsulated in a benzocyclobutene (BCB) polymer matrix for ensuring their mechanical stability. The BCB matrix was etched by reactive ion etching and chemical HCl etching to expose the top surface of the NWs for further accessibility to electrically contact them during AFM conductivity measurements.

2.2.2. GaAs NW PIN junction nanowires. Axial GaAs PIN junctions were fabricated on Si N+ substrates by opening and closing the shutter appropriately during the growth. A 200 nm long section was incorporated between the p- and n-doped regions to favour carrier separation. Fig. 3 illustrates the design of two samples fabricated with PIN structures, and a typical SEM picture. The first sample was fabricated without passivation while the second was passivated using a 10 nm AlGaAs layer, as illustrated in the schematic representation in Fig. 3a. Both samples were grown on Si(111) N+ substrates, starting with the N segment including GaAs and a vapor of Te (the GaTe cell temperature was 450 °C), for 12 minutes. Then, the Te shutter was closed, and the GaAs continued growing for 2.5 minutes resulting in an intrinsic segment. Subsequently, the Be shutter was opened for 4.5 minutes to form the P-doped segment (the Be cell temperature was 850 °C). Finally, the Ga droplet catalyst was consumed, and then radial growth was performed to protect the III–V nanowire facets and avoid surface recombination, and this was achieved by growing an AlGaAs shell at 400 °C for 4 minutes on one of the two samples.

3. Results and discussion

3.1. Morphological investigation of embedded PIN GaAs nanowires

The NW surface morphology was measured using a metrological AFM (NX20, Park Systems, Republic of Korea) in intermittent contact mode using an aluminium coated, high resonance frequency silicon probe with nominal $f_{resonance}$ = 330 kHz, k = 42 N m^{-1}, guaranteed AFM tip radius of curvature <10 nm and a scan rate set to 0.2 Hz (PPP-NC-HR, Nanosensors, Switzerland) to help unveil the sample's structure. This type of experiment was previously conducted to assess various nanowire characteristics including, but not limited to, dimensions, side-wall roughness, periodicity, and defects.[22] In this study, we have selected a challenging sample to test the power and flaws of diverse probing methods. The sample is composed of vertically aligned p-type GaAs nanowires which were embedded

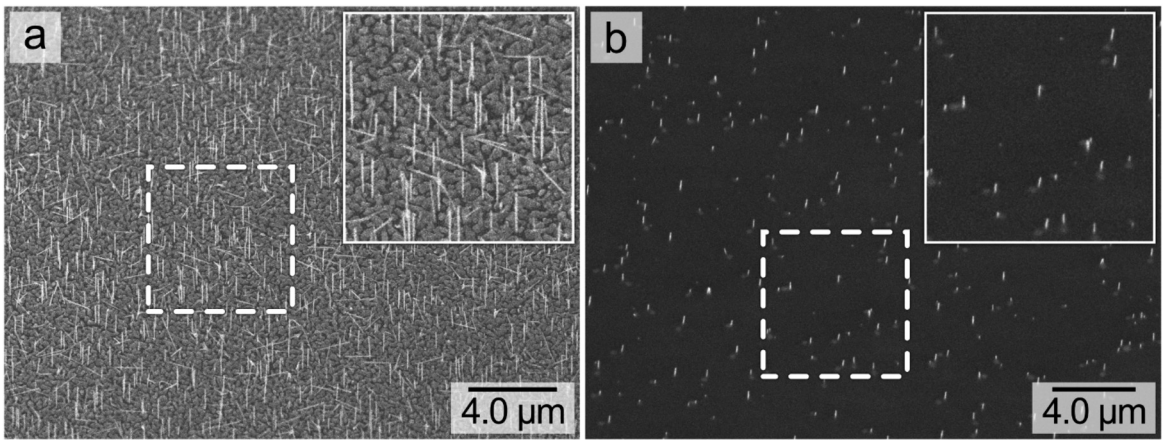

Fig. 2 SEM images of p-type GaAs NWs after the VLS growth (a) and after the BCB encapsulation and reactive ion etching revealing their upper part (b).

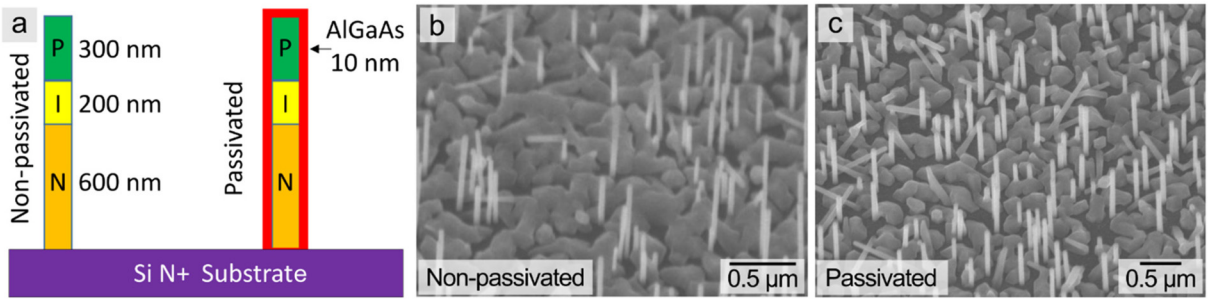

Fig. 3 (a) Drawings and (b and c) SEM images of non-passivated and passivated GaAs NWs with PIN axial junctions.

in a benzocyclobutane (BCB) polymer matrix after growth for structural support and then etched to expose the nanowires.

Due to the oxidizing nature of the GaAs surface, the sample was thoroughly cleaned prior to scanning. This enables the selection of appropriate areas on the sample surface to measure further in AFM electrical modes (*e.g.*, C-AFM measurements). Non-periodic nanowires with differing heights are observed in Fig. 4a which is a 20 × 20 μm^2, 512 × 512 pixel image, providing essential information about the nanowires' alignment, exposure, and mechanical stability post-etching. Three different groups of nanowires are observed contributing to the topography: (1) fully exposed nanowires sticking out of the polymer matrix, (2) partially exposed or just below the surface nanowires, and (3) deeply embedded nanowires. This is illustrated by a cartoon in Fig. 4b. A detailed look at a 5 × 5 μm^2, 512 × 512 pixel image, rendered in 3D (Fig. 4c), helps identify individual nanowires sticking out of the polymer matrix, and others exhibiting various degrees of closeness to the surface. The variation in NW height and nearest-neighbour distancing result in different degrees of exposure, directly impacting the electrical measurements. Some NWs may not be sufficiently exposed to conduct electric current, while some NWs may be too tightly packed for single-entity spectroscopy, affecting device performance and reproducibility.

3.2. EFM investigation of embedded PIN GaAs nanowires

Electrostatic force microscopy (EFM) measurements were performed using a platinum/iridium-coated silicon probe with $f_{resonance}$ = 140 kHz, k = 7.4 N m^{-1} (PPP-NCSTPt, Nanosensors, Switzerland). Conductive AFM probes enable the measurement of electrostatic force variations resulting from the charged nature of sample's nanostructures. Fig. 5a shows a 20 × 20 μm^2, 512 × 512 pixel image of non-passivated GaAs nanowires imaged in double-pass EFM mode at a scan rate set to 0.2 Hz, an amplitude set point of 47 nm, and a lift height of 10 nm. Owing to the extreme surface sensitivity of this mode, the bright spots on the EFM amplitude map (Fig. 5b) reveal the signature of the nanowires sticking out of the BCB matrix as charges accumulate on them. Although the remaining nanowires show contrast variation on the surface topography map (Fig. 5a and c), only some of the fully exposed and partially protruding ones contribute to direct changes in the electrostatic force measurements with differences in individual NW charge contributions (Fig. 5b and c). In addition to probing the electrically charged nature of the nanowires, fast, intermittent contact EFM measurements provide means to investigate the surface distribution of exposed nanowires and their qualitative contribution to surface potential, which is crucial for further spectroscopic measurements requiring direct contact

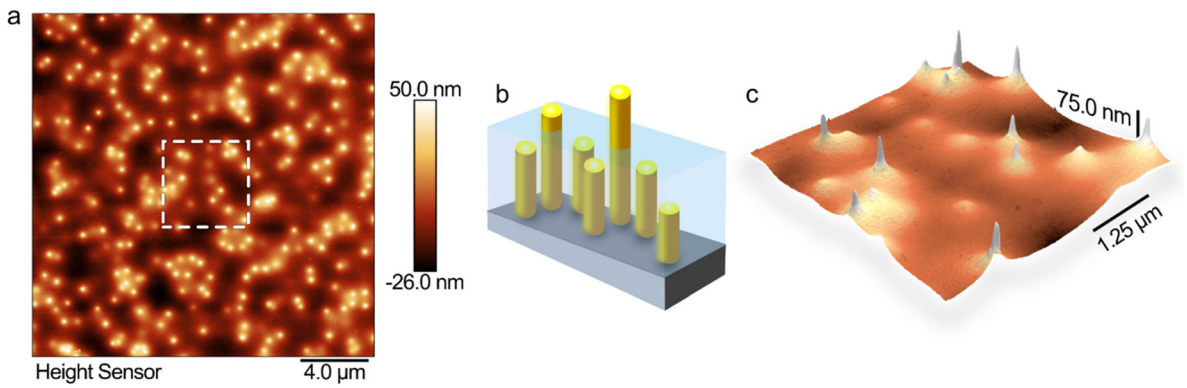

Fig. 4 (a) A 20 × 20 μm^2 AFM topography image of p-type GaAs nanowires embedded in a BCB polymer matrix and then etched. (b) Schematic illustration of the embedded nanowires highlighting the exposure of some nanowires while the remaining ones exhibit different degrees of closeness to the matrix's top surface. (c) 3D rendering of the surface topography from a 5 × 5 μm^2 scan (dashed white square), showing various nanowires sticking out of the polymer matrix, with others still fully embedded under the surface.

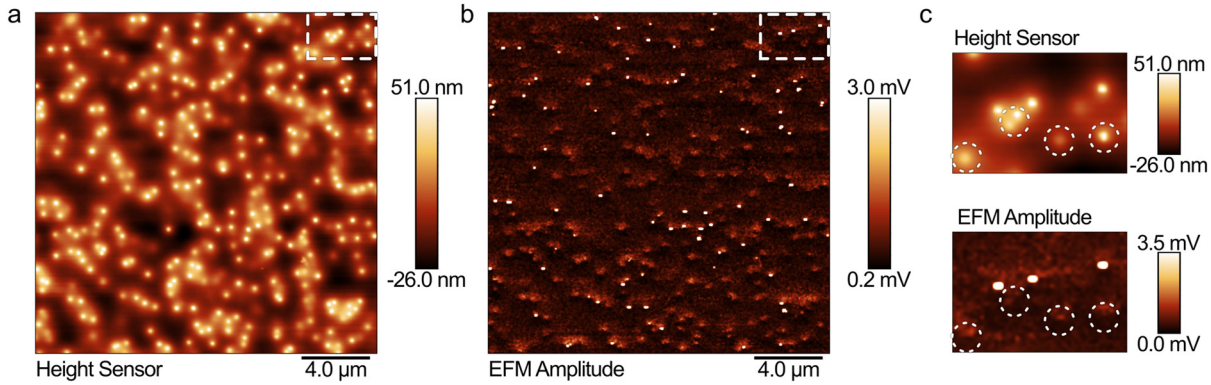

Fig. 5 EFM measurements of non-passivated GaAs nanowires embedded in a BCB polymer matrix, (a) showing the sample's topography and (b) the variations in the EFM amplitude of the electrostatically driven oscillating cantilever. The difference in individual NW contributions to surface charge is highlighted in (c).

between the AFM tip and the top surface of individual nanowires.

3.3. KPFM investigation of embedded PIN GaAs nanowires

Kelvin probe force microscopy (KPFM) extends over EFM measurements by quantifying the surface potential through the measurement of the contact potential difference (CPD) using an additional feedback loop to minimize the electrostatic forces stemming from work function differences between the tip and the sample. The KPFM method features numerous operating variations enabling surface topography measurements either in intermittent contact or peak force (PF) tapping™ modes, and surface potential measurements either in amplitude modulation (AM) or frequency modulation (FM) schemes.[23,24] Here, we conducted KPFM measurements on arrays of non-passivated GaAs PIN junction NWs by the PF KPFM approach (Fig. 6) on a Dimension Icon system (Bruker, USA) using a conductive platinum/iridium-coated silicon probe (SCM PIT-V2, Bruker, USA), with k = 2.93 N m^{-1}, determined using the thermal tune method, a 75 kHz fundamental resonance frequency, a 25 nm nominal tip radius, and a lift height of 50 nm. This operating mode consists of measuring the surface topography and mechanical properties in the peak force quantitative nanomechanical mapping (PF QNM™)

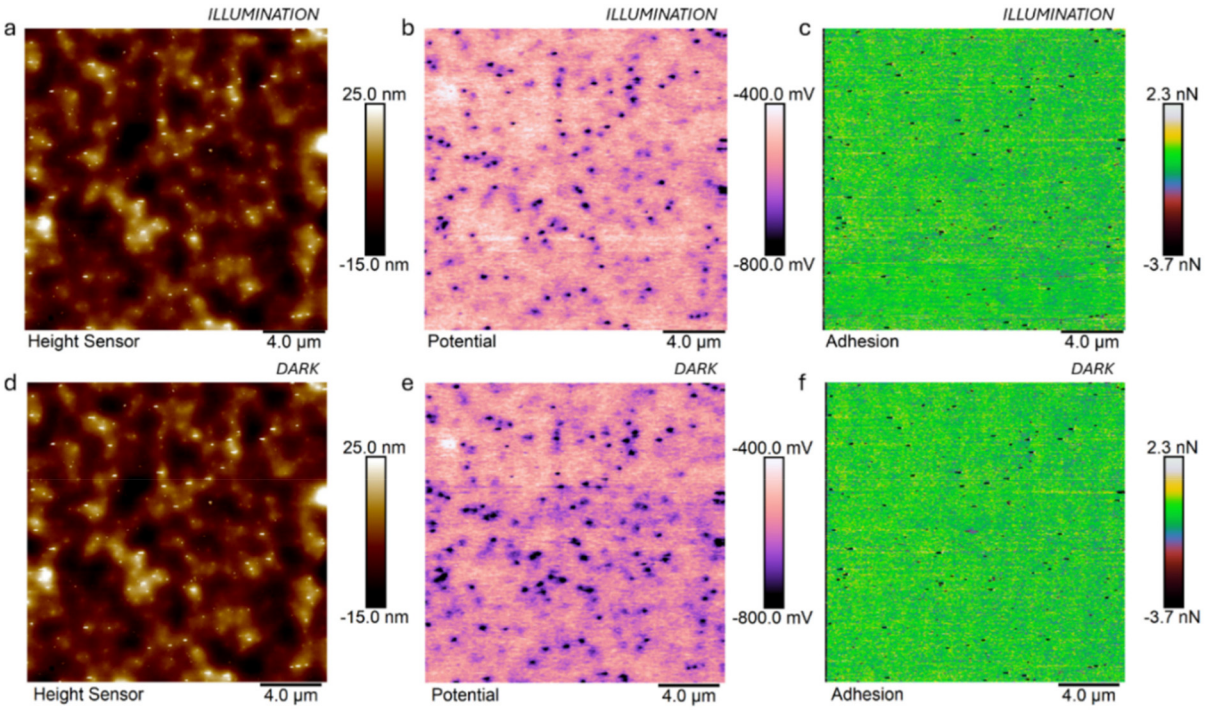

Fig. 6 (a–c) Topography, surface potential, and adhesion maps, respectively, measured in PF KPFM under illumination conditions on the sample of non-passivated vertical nanowire array (non-passivated). (d–f) Same measurements performed under dark conditions.

mode and the surface potential in FM mode.[25] Experiments were performed in the dark and under illumination environmental conditions to investigate possible changes in the photovoltaic properties of the nanowires. The difference in CPD measured under illumination and in the dark corresponds to the surface photovoltage, which can be correlated to the open-circuit voltage, V_{oc}.

Fig. 6 shows the surface topography (a and d) of the sample correlated to surface potential (b and e) and adhesion (c and f) maps under illumination (top row) and dark (bottom row) conditions. The surface potential maps (b and e) show a dark contrast corresponding to the surface potential of the nanowires measured in KPFM. Remarkably, not all nanowires observed on the surface topography maps (a and d) show a surface potential contrast (b and e). Moreover, the measured nanowires exhibit different contrast levels on the surface potential maps. This observation aligns well with the observations in EFM measurements (Fig. 5), indicating the dependence of the nanowires' electrostatic signature on their vertical level inside the polymer matrix (*i.e.*, protruding or embedded – Fig. 4). More importantly, the simultaneous measurement of the mechanical properties in the PF KPFM mode enables the mapping of the tip–sample adhesion, as shown in Fig. 6(c and f). Owing to the extreme surface sensitivity of the measured adhesion between the tip apex and the top surface of the sample, only the exposed (sticking out from the matrix) nanowires appear as dark dots in Fig. 6(c and f). Therefore, PF KPFM offers a valuable means to unveil correlated information on the structural and electrical properties of the nanowires in the polymer-embedded array.

Fig. 7 summarizes the CPD measurements performed on individual non-passivated PIN devices (with mapping shown in Fig. 6) and passivated PIN devices (mapping not shown) under both dark and illumination conditions (Fig. 7a and c). It also presents the CPD differences between these two conditions (Fig. 7b and d). The results show that the nanowires exhibit ΔPD = 93.3 mV and ΔCPD = 126.1 mV for non-passivated and passivated samples, respectively. These values indicate small V_{OC} values in both cases under white LED illumination from the AFM microscope, with the passivated nanowires exhibiting an ≈ 30 mV higher ΔCPD value than the non-passivated ones. It is worth noting that the absence of passivation exposes the top surface of the nanowires sticking out of the matrix to air, which induces GaAs oxidation effects.

3.4. C-AFM investigation of embedded PIN GaAs nanowires

The top surface oxidation of the non-passivated nanowires is directly probed in conductive-AFM (C-AFM) measurements using a conductive doped diamond probe (AD2.8AS, Adama Innovations, Ireland) in contact with the sample surface. By applying a bias voltage (V_{bias}) between the tip and the sample, the current flowing through the nanowires is measured. Current maps and current *versus* voltage (*I–V*) curves could be obtained in C-AFM scanning and spectroscopic modes, respectively.[26–29]

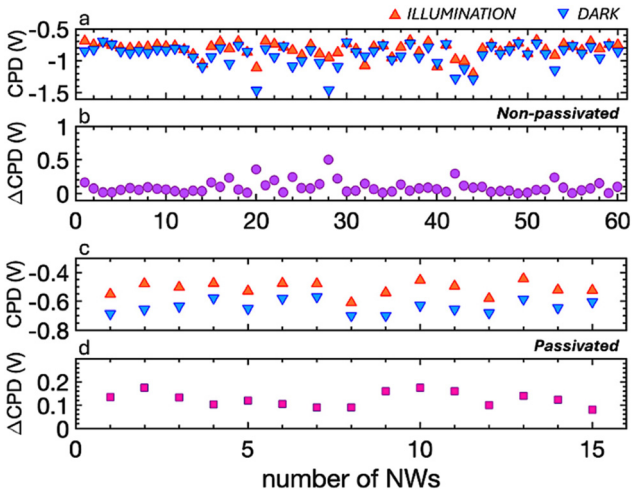

Fig. 7 Contact potential difference (CPD) values measured on individual non-passivated (a) and passivated (c) nanowires under illumination and dark conditions. The differences in CPD (b and d) are determined for each nanowire between the measurements under these two conditions.

Initial measurements on the non-passivated GaAs nanowires revealed a lack of conductivity (*i.e.*, zero current) due to the oxidation of the nanowires' top surface. Consequently, a surface treatment protocol was devised for oxide removal, consisting of the following steps. First, the nanowire sample is immersed in boiling acetone (65 °C for 5 minutes) and then in boiling methanol (65 °C for 5 minutes). Finally, the sample is immersed in concentrated HCl for 30 seconds. Deionized water is used for rinsing the sample after each step.

Subsequently, C-AFM imaging measurements were carried out, enabling the correlation between the surface topography and electrical conductivity maps at various locations, as shown in Fig. 8. The C-AFM imaging results reveal a series of important information, as follows. First, all current maps (Fig. 8(b, c, e and f)) demonstrate that only a small number of nanowires in the array (*i.e.*, compared to the number of nanowires observed on the topography map) are conductive. This provides highly valuable insights into the conductivity distribution across the nanowire arrays, which is key to dictating their functional performance when integrated in full devices. Access to this information unlocks direct means to assess the effectiveness of nanowire fabrication procedures and growth conditions. Second, the current maps show some nanowires (highlighted with blue dashed squares) that yield high current values independently of the bias or illumination conditions. This points toward failed nanowires, which do not exhibit any semiconducting properties.

Third, the comparison between the current maps in Fig. 8 (b and e) reveals the effect of illumination on the potential photovoltaic behaviour of the nanowires. When a V_{bias} = 2 V is applied between the tip and the sample, several nanowires are consistently observed conducting current under dark and illumination conditions, which indicates a non-photovoltaic

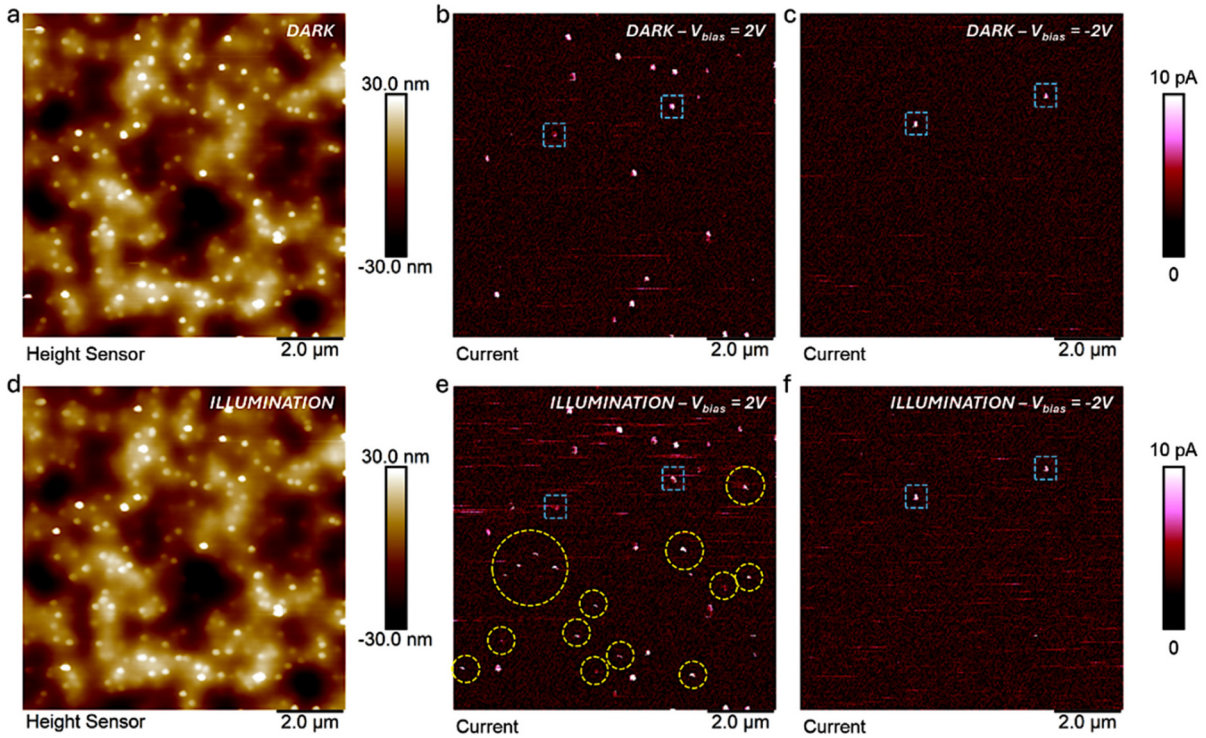

Fig. 8 C-AFM measurements of non-passivated GaAs NWs under dark and under illumination conditions showing (a and d) the surface topography maps and current maps measured with an applied V_{bias} = 2 V (b and e) and V_{bias} = −2 V (c and f).

behaviour. Nevertheless, these same nanowires disappear from the current maps acquired at a V_{bias} = −2 V, which points towards a diode-like behaviour of these nanowires. Interestingly, additional nanowires (highlighted with yellow dashed circles in Fig. 8e) only appear on the current map under illumination at V_{bias} = 2 V, which is a signature of their photovoltaic behaviour. All of the above results put forward the non-homogeneity of the nanowires' behaviour across the array, which promotes the importance of their nanoscale characterization in correlative AFM modes to deepen the insight into individual nanowires' properties affecting the overall photovoltaic devices.

The aforementioned observations are further confirmed *via* *I–V* measurements performed by contacting individual nanowires within the array with the conductive AFM tip. Fig. 9a shows an example of a non-responsive wire with a flat *I–V* curve, while the *I–V* curves of electrically responsive nanowires are shown in Fig. 9(b–d). Black curves are recorded during the forward sweep (*i.e.*, rising bias voltage), whereas red curves correspond to the backward sweep (*i.e.*, dropping bias voltage). Surprisingly, the black and red curves do not overlap, which raises several questions, in particular whether the first voltage sweep induces a change in the mechanical/electrical properties of the nanowire. Nevertheless, we can still observe a diode behaviour (black curve) and a pseudo-photovoltaic effect (red curve). Indeed, the pseudo photovoltaic effect points out a V_{OC} with no short-circuit current I_{SC}. However, the loss of mechanical/electrical contact between the AFM tip and the device

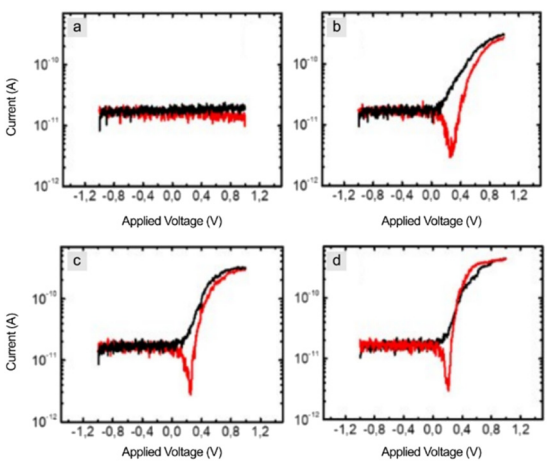

Fig. 9 Current *versus* voltage (*I–V*) curves measured by contacting individual nanowires across the array. (a) Example of a non-responsive nanowire. (b–d) Electrically responsive nanowires showing diode-like and pseudo-photovoltaic behaviours. Black lines correspond to the forward sweep of the bias (increasing voltage) and red lines correspond to the reverse sweep.

could be wrongly interpreted as an open-circuit device. Furthermore, it should be noted that there is likely an AFM tip shadowing effect, which could influence the *I–V* measurement procedure. In general, the illumination reaching the nanowire device is not well-defined, as it primarily comes from multiple possible sources, including the LED microscope light and the

alignment laser. Additionally, the size of the AFM tip may impact the illumination perceived by the nanodevice.[30,31]

Although the *I–V* curve measurements correlate well with the C-AFM and KPFM imaging results, they highlight the challenges associated with single-entity *I–V* spectroscopy of nanoscale structures under varying environmental conditions. Identifying the reasons for the disparity between *I–V* curves calls for a significantly large number of experimental data collected over a large number of single entities.

4. Conclusions

This study highlights the exceptional versatility and efficacy of the AFM as a multimetrological platform for the comprehensive morphological, electrical, and spectroscopic characterization of optical nanomaterials under different environmental conditions at the nanoscale. Through the synergistic application of EFM, KPFM, and C-AFM modes on nanowires, we have demonstrated the capability to probe diverse nanoelectrical properties with precision and high resolution.

The ability to easily switch between various modes of characterization positions the AFM as a cornerstone in metrological applications for a comprehensive understanding of novel energy harvesting devices and nanomaterials.

Future research in this field can further explore the potential of AFM as a multimetrological platform by integrating emerging technologies such as AFM-IR.[32,33] This combination allows nanoscale chemical characterization by coupling infrared spectroscopy with AFM's spatial, electrical, and mechanical modes.

Author contributions

HA, KK, JMM, FP, JA, NC, JP, SMS and PR have contributed to conceptualization, data acquisition, curation and analysis. HA and FP further contributed to funding acquisition, project administration, supervision and writing the original draft. In addition, KK and SMS contributed to writing – review & editing.

Data availability

All data supporting this article have been published online at **https://doi.org/10.5281/zenodo.14271622**.

Conflicts of interest

There are no conflicts to declare.

Acknowledgements

This research project is supported by the European Union and is funded within the scope of the European Metrology Programme for Innovation and Research (EMPIR) project 19ENG05 NanoWires entitled 'High throughput metrology for nanowire energy harvesting devices' (**https://www.ptb.de/empir2020/%20nanowires/home/**). Further funding has been provided by the Horizon Europe Marie Skłodowska-Curie Actions project 101086226 ENSIGN - 'Emerging nanoscopy for single entity characterization'. (**https://cordis.europa.eu/project/id/101086226**), and both projects were co-financed by the Danish Ministry of Higher Education and Science. The authors thank the NanoLyon platform for access to equipment and J. B. Goure for technical assistance.

References

1 F. J. Giessibl, *Rev. Mod. Phys.*, 2003, **75**, 949–983.
2 S. Hoffmann, I. Utke, B. Moser, J. Michler, S. H. Christiansen, V. Schmidt, S. Senz, P. Werner, U. Gösele and C. Ballif, *Nano Lett.*, 2006, **6**, 622–625.
3 Y. Coffinier, S. Janel, A. Addad, R. Blossey, L. Gengembre, E. Payen and R. Boukherroub, *Langmuir*, 2007, **23**, 1608–1611.
4 X. Wang, J. Song and Z. L. Wang, *J. Mater. Chem.*, 2007, **17**, 711–720.
5 D. Mikulik, M. Ricci, G. Tutuncuoglu, F. Matteini, J. Vukajlovic, N. Vulic, E. Alarcon-Llado and A. Fontcuberta i Morral, *Nano Energy*, 2017, **41**, 566–572.
6 S. H. Pham, A. Ferri, A. Da Costa, M. M. S. Mohan, V. D. Tran, D. C. Nguyen, P. Viville, R. Lazzaroni, R. Desfeux and P. Leclère, *Adv. Mater. Interfaces*, 2022, **9**, 2200019.
7 W. Hourani, B. Gautier, L. Militaru, D. Albertini and A. Descamps-Mandine, *J. Vac. Sci. Technol., B:Nanotechnol. Microelectron.:Mater., Process., Meas., Phenom.*, 2011, **29**, 01AA06.
8 G. Paul, *Nanotechnology*, 2001, **12**, 485.
9 X. Qian, Z. Lin, L. Guan, Q. Li, Y. Wang, M. Zhang and M. Dong, *Nanoscale Res. Lett.*, 2017, **12**, 257.
10 D. Nunes, T. R. Calmeiro, S. Nandy, J. V. Pinto, A. Pimentel, P. Barquinha, P. A. Carvalho, J. C. Walmsley, E. Fortunato and R. Martins, *Thin Solid Films*, 2016, **601**, 45–53.
11 H. M. Singh, B. Choudhuri and P. Chinnamuthu, *IEEE Trans. Nanotechnol.*, 2020, **19**, 628–634.
12 A. Karbassi, D. Ruf, A. D. Bettermann, C. A. Paulson, D. W. van der Weide, H. Tanbakuchi and R. Stancliff, *Rev. Sci. Instrum.*, 2008, **79**, 094706.
13 H. P. Huber, M. Moertelmaier, T. M. Wallis, C. J. Chiang, M. Hochleitner, A. Imtiaz, Y. J. Oh, K. Schilcher, M. Dieudonne, J. Smoliner, P. Hinterdorfer, S. J. Rosner, H. Tanbakuchi, P. Kabos and F. Kienberger, *Rev. Sci. Instrum.*, 2010, **81**, 113701.
14 J. Hoffmann, G. Gramse, J. Niegemann, M. Zeier and F. Kienberger, *Appl. Phys. Lett.*, 2014, **105**, 013102.
15 S. Hommel, N. Killat, A. Altes, T. Schweinboeck and F. Kreupl, *Microelectron. Reliab.*, 2017, **76–77**, 218–221.

16 M. C. Biagi, G. Badino, R. Fabregas, G. Gramse, L. Fumagalli and G. Gomila, *Phys. Chem. Chem. Phys.*, 2017, **19**, 3884–3893.
17 A. Buchter, J. Hoffmann, A. Delvallée, E. Brinciotti, D. Hapiuk, C. Licitra, K. Louarn, A. Arnoult, G. Almuneau, F. Piquemal, M. Zeier and F. Kienberger, *Rev. Sci. Instrum.*, 2018, **89**, 023704.
18 D. Richert, J. Morán-Meza, K. Kaja, A. Delvallée, D. Allal, B. Gautier and F. Piquemal, *Nanomaterials*, 2021, **11**, 3104.
19 W. Choi, E. Seabron, P. K. Mohseni, J. D. Kim, T. Gokus, A. Cernescu, P. Pochet, H. T. Johnson, W. L. Wilson and X. Li, *ACS Nano*, 2017, **11**, 1530–1539.
20 B. A. Joyce, *Rep. Prog. Phys.*, 1985, **48**, 1637.
21 T. Mårtensson, M. Borgström, W. Seifert, B. Ohlsson and L. Samuelson, *Nanotechnology*, 2003, **14**, 1255.
22 H. J. Yun, S. J. Kim, J. H. Hwang, Y. S. Shim, S. G. Jung, Y. W. Park and B. K. Ju, *Sci. Rep.*, 2016, **6**, 34150.
23 K. Kaja, A. Assoum, P. De Wolf, F. Piquemal, A. Nehmee, A. Naja, T. Beyrouthy and M. Jouiad, *Adv. Mater. Interfaces*, 2024, **11**, 2300503.
24 K. Kaja, D. Mariolle, N. Chevalier, A. Naja and M. Jouiad, *Rev. Sci. Instrum.*, 2021, **92**, 023703.
25 B. Pittenger, N. Erina and C. Su, *Bruker application note AN128, Rev*, Bruker, 2012.
26 A. Stern, S. Aharon, T. Binyamin, A. Karmi, D. Rotem, L. Etgar and D. Porath, *Adv. Mater.*, 2020, **32**, 1907812.
27 A. Alexeev, J. Loos and M. M. Koetse, *Ultramicroscopy*, 2006, **106**, 191–199.
28 F. Giannazzo, E. Schilirò, G. Greco and F. Roccaforte, *Nanomaterials*, 2020, **10**, 803.
29 H. Si, S. Zhang, S. Ma, Z. Xiong, A. Kausar, Q. Liao, Z. Zhang, A. Sattar, Z. Kang and Y. Zhang, *Adv. Energy Mater.*, 2020, **10**, 1903922.
30 C. Marchat, L. Dai, J. Alvarez, S. Le Gall, J.-P. Kleider, S. Misra and P. Roca i Cabarrocas, *Nanoscale Res. Lett.*, 2019, **14**, 398.
31 R. Khoury, J. Alvarez, T. Ohashi, I. Martín, P. Ortega, G. López, C. Jin, Z. Li, Rusli, P. Bulkin and E. V. Johnson, *Nano Energy*, 2020, **76**, 105072.
32 A. Dazzi and C. B. Prater, *Chem. Rev.*, 2017, **117**, 5146–5173.
33 A. Dazzi, C. B. Prater, Q. Hu, D. B. Chase, J. F. Rabolt and C. Marcott, *Appl. Spectrosc.*, 2012, **66**, 1365–1384.